CHARACTERIZATION OF THz RADIATION AT FLUTE

J. Schaefer*, M. Brosi, E. Bründermann, A. Malygin, A.-S. Müller, M. J. Nasse,
R. Ruprecht, M. Schuh, M. Schwarz, N. Smale, J. L. Steinmann
Karlsruhe Institute of Technology (KIT), Karlsruhe, Germany

Abstract

FLUTE, the Ferninfrarot Linac- und Test-Experiment at KIT, is a compact linac-based accelerator test facility and provides electron bunch energies up to several tens of MeV with a wide range of charges. A bunch compressor allows tuning the bunch length from picoseconds down to the femtosecond-scale. FLUTE can therefore generate short, intense THz radiation for a wide variety of applications. In this contribution, we report on the characterization measurements of THz radiation generated after the bunch compressor.

SETUP

In this paper, we present first THz measurements generated by the FLUTE high-energy section and attempts to separate synchrotron radiation, edge radiation, and transition radiation. First THz emission using the FLUTE low-energy section was measurement last year [1]. At FLUTE [2] electrons are generated and pre-accelerated to 5 MeV in the low-energy section and then brought to 42 MeV by an S-band linac. A four-dipole bunch compressor (BC) allows compressing the bunch longitudinally. We used a quadrupole triplet between linac and BC to focus the beam transversely at the plane of an aluminum foil. The foil is installed at 45° to the beam axis and reflects radiation by 90° toward an extraction window and detector.

The measured radiation can be a combination from three different sources: Synchrotron radiation (SR) is emitted as the beam traverses the dipole bends, and edge radiation (ER) arises from the region of a sharp change in magnetic field at the entrance and exit faces of the rectangular dipole poles. Both SR and ER are reflected off the foil toward the detector. For geometric reasons, the strongest ER reaching the detector is mainly emitted from the last dipole exit face, other edges contribute partially, depending on the set BC deflection angle. The beam also produces transition radiation (TR) upon interaction with the foil, which is directed toward the same detector.

The detector, shown in Fig. 1, consists of four Schottky barrier diode detectors with horn antennas, sensitive at center frequencies of 272, 412, 625 and 925 GHz (± 20 % bandwidth each), referred to as M1–M4. The sensors are mounted on a *yz*-translation stage and arranged with a minimum spacing of 22 mm. This is a common bunch compression monitoring diagnostic, presented for instance in [3]. This arrangement allows for simultaneous coarse measurement of the radiation spectrum with all four diodes without repositioning the detectors. The diodes are linearly polarized; adjacent diodes have orthogonal polarization axes, an unavoidable consequence of the compact geometry, as visible in Fig. 1. The complete assembly can rotate to 0°, 45° and 90° about the center point of the four sensors to probe different polarization projections. Each diode is connected directly to an oscilloscope channel (2 GHz bandwidth, 12-bit native resolution). For each bunch passage, the oscilloscope extracts the extreme value in the time domain per diode channel. The Schottky type diodes yield negative signals when excited, thus the data shown are given as negative voltages. Absolute signal amplitudes between diodes are not directly compared as the individual diode scaling factors are not calibrated.

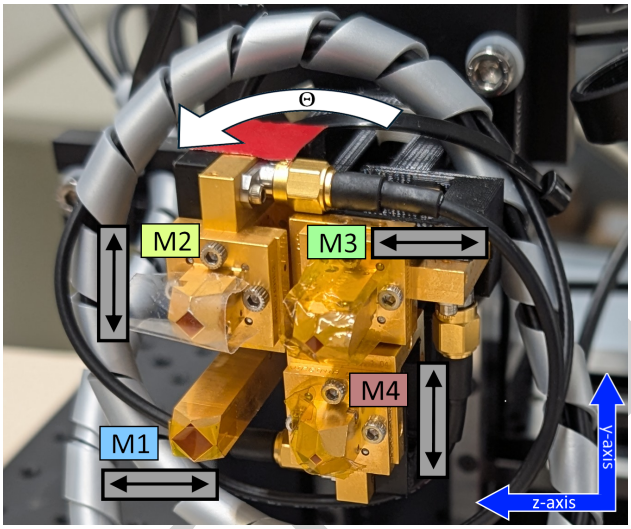

Figure 1: Photograph of the four-diode THz detector assembly. Sensors M1–M4 are arranged with minimal spacing; adjacent diodes have alternating linear polarization axes, as indicated by the gray arrows. The detector can rotate about the center point by Θ and translates in the two transverse directions of the radiation axis *y* and *z*. The photo was taken at Θ = 0°. The tape on-top of the diodes antennas serve as dust protection and is transparent to the measured radiation.

EXPECTED RADIATION SPECTRA

The intensity per frequency f and solid angle Ω interval emitted by a bunch of N electrons is [4]

$$\frac{\mathrm{d}^2 I_i}{\mathrm{d}f\,\mathrm{d}\Omega} = \left[N + N^2\,|F(f)|^2\right] \cdot SPE_i(f,\Omega)\ , \qquad (1)$$

where SPE_i is the single-particle emission spectrum for the individual radiation type $i \in \{\mathrm{ER}, \mathrm{SR}, \mathrm{TR}\}$. For FLUTE, the SPE for ER and SR are discussed in detail in [5] and for TR in [6]. Because the three types have distinct polarisation and angular emission patterns, the linearly polarised diodes

* jens.schaefer2@kit.edu

and the rotatable detector assembly have the potential to separate the signal contributions. Here, we focus on the experimentally measured signals, which represent the sum of all three types.

The scaling in Eq. (1) is identical across all radiation types. The first term describes incoherent radiation scaling with N; the second is the coherent contribution, scaling with N^2 and the longitudinal bunch form factor

$$|F(f)|^2 = \exp\left[-(2\pi f\, \sigma_t)^2\right], \tag{2}$$

with the rms bunch duration σ_t, which is the Fourier transform of the longitudinal line-density profile of a Gaussian bunch.

The experiments were conducted at a bunch charge of 17 pC, corresponding to $N \approx 10^8$ electrons, enhancing the coherent term by up to eight orders of magnitude over the incoherent signal.

The coherence condition $|F(f_{\mathrm{coh}})|^2 = 1/e$ defines a critical frequency, below which the signal is strongly increased, see Table 1. Note that the coherent emission is scaled by the form factor shown in Fig. 2 and even small form factor values allow for a strong coherent enhancement due to the large number of electrons in the bunch. For FLUTE, simulations suggest single-digit femtoseconds for an ideal match of a (h, R_{56}) combination [7], these quantities are explained below.

Table 1: Diode Frequencies and Required Bunch Duration σ_t for the Coherence Condition $|F|^2 = 1/e$

Diode	f [GHz]	σ_t for $\lvert F\rvert^2 = 1/e$
M1	272	585 fs
M2	412	386 fs
M3	625	255 fs
M4	925	172 fs

The form factor $|F(f)|^2$ calculated for some example bunch lengths including the values from Table 1 are displayed in Fig. 2. The sensitive frequency bands of the four diodes are indicated by the coloured regions. Depending on the bunch length, the coherent enhancement reaches different sensors: a shorter bunch shifts the form factor to higher frequencies, bringing higher-frequency diodes into the coherent regime.

EXPERIMENT

Two degrees of freedom control the bunch length at FLUTE. The linac RF phase φ sets the energy chirp h of the bunch, the longitudinal energy–position correlation:

$$h = \frac{\mathrm{d}E}{\mathrm{d}z} \propto \tan(\varphi)\,. \tag{3}$$

The BC deflection α sets the compression factor via the transport matrix element $R_{56} \propto \alpha$ [8]. Lower-energy electrons travel a longer path and arrive later, compressing the longitudinal phase space when h and R_{56} are well matched.

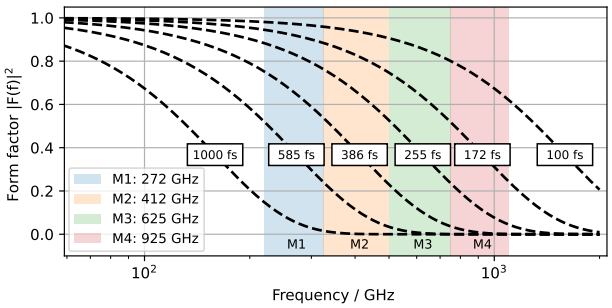

Figure 2: Form factor $|F(f)|^2$ for different bunch lengths of Gaussian shape. The colored bands indicate the 20% spectral sensitivity range of the four diodes M1–M4.

$\varphi = 0°$ (on-crest) gives maximum energy gain and zero chirp; larger $|\varphi|$ increases $|h|$ monotonically. A mismatch between h and R_{56} results in under- or over-compression and thus in a longer bunch with lower coherent signal.

Bunch Length Scan

The RF phase φ was stepped from 0° to 52° in 16 steps. To maintain a constant mean bunch energy of 42 MeV, the linac power was increased simultaneously. In addition α was varied from 0° to 14° in 8 steps. The quadrupole triplet was re-optimised at each α step to maintain a comparable beam size at the foil. Mean energy, beam size and charge were held stable, only the longitudinal profile changed. The detector was positioned such, that all four diodes are illuminated simultaneously. The detector was rotated to $\Theta = 45°$ to sample horizontal, vertical and diagonal polarization components.

Figure 3 shows the diode signals versus φ, with α encoded by colour. For each α an optimal φ produces a short bunch; the signal peaks sharply and falls as the bunch leaves the coherent regime. The peak φ shifts to larger offsets with increasing α, consistent with the larger R_{56} requiring a stronger chirp to yield a short bunch. Above $\varphi \approx 30°$ the peak phase becomes less consistent across diodes, reflecting nonlinear longitudinal dynamics at increased energy spread.

Three features stand out. First, the coherent signal window narrows from M1 to M4, as signals at higher frequencies require shorter bunches achievable over a narrower φ range.

Second, M1 and to some extent M2 behave anomalously, with signals increasing monotonically with φ and favouring low α, inconsistent with bunch compression. As the DAQ extracts only the minimum peak value per bunch without timing discrimination, contributions from dark current or reflections may falsify measurements. This could be a possible explanation for the lowest frequency diode M1 yielding different trends than the other diodes.

Third, M4 shows the clearest compression signature: the strongest signal at $\varphi = 43°$ and $\alpha = 6°$ stands out clearly from the rest of the dataset. This is consistent with this operating point corresponding to the shortest bunch of the scan. While for all other (φ, α) combinations the coherence condition is met for M1, M2 and M3, it is not met for M4; M4 is excited by coherently enhanced radiation only for the

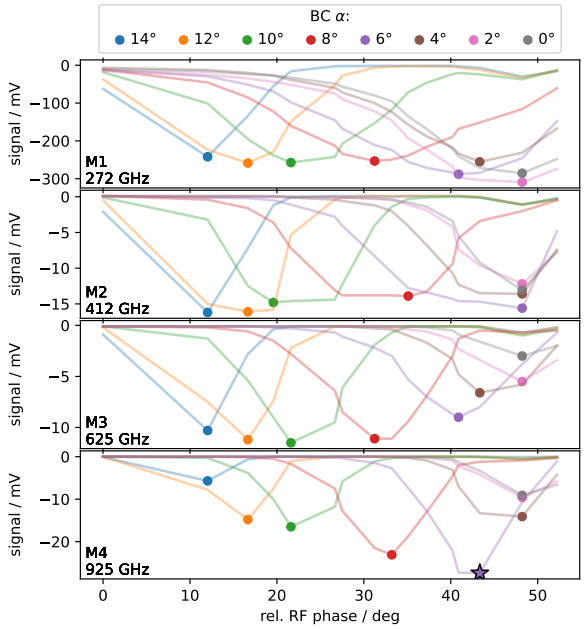

Figure 3: Diode signals M1–M4 vs. RF phase φ. Colors indicate BC deflection α from 0° (grey) to 14° (blue); filled circles mark the minimum per α. The strongest M4 signal at $\varphi = 43°$ and $\alpha = 6°$ indicates the shortest measured bunch, marked by a star.

shortest bunch. This explanation places the bunch length near 172 fs.

Transverse Plane Scan

At the working point of maximum signal of M4 ($\varphi = 43°$, $\alpha = 6°$) the detector was scanned in the horizontal (z) and vertical (y) directions transverse to the radiation axis. The scan was repeated at detector rotations $\Theta = 0°$ and $\Theta = 90°$ to probe orthogonal polarisation projections; the bunch length scan was conducted at $\Theta = 45°$ to sample both components, simultaneously.

Figure 4 shows the normalized intensity maps for all diodes at both rotations. The 22 mm diode spacing is visible as an offset between subplots; the shift in diode positions upon rotation by 90° can be followed across the rows. The polarisation axis of is indicated by a white arrow.

ER and TR both produce a doughnut-shaped emission pattern [9] with a central null on the beam axis, both patterns carry radial polarisation. Because each diode is sensitive only to linear polarisation, it projects the radially polarised ring onto a single direction, selecting one hemisphere and suppressing the opposite side. Rotating the detector by 90° flips the selected hemisphere. This is clearly visible in the two rows of Fig. 4. SR, by contrast, produces a forward lobe with a maximum on the beam axis, this serves for one possible explanation for the non-zero intensity at the pattern centre. The overall pattern size decreases from M1 to M4, this is consistent with the prediction in [6]. The M4 maps appear to be affected by saturation in the highest-intensity regions.

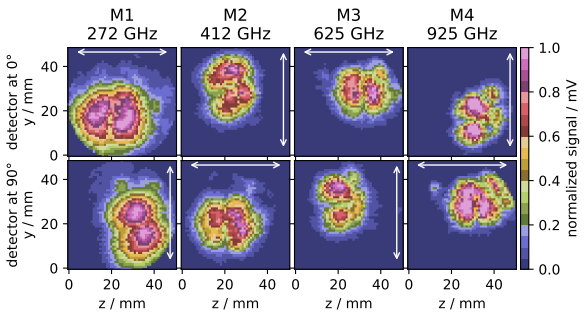

Figure 4: Transverse intensity maps at detector rotations $\Theta = 0°$ (top) and 90° (bottom) for diodes M1–M4. Axes give the detector position in mm. Each subplot is normalised to its own maximum. White arrows indicate the linear polarisation axis of each diode. The 22 mm diode spacing and its rotation-induced shift are visible as offsets between subplots.

Separation of the Radiation Types

An attempt to separate the radiation types exploits the fact that SR and ER are emitted in the BC dipoles and are unaffected by where the beam strikes the foil, whereas TR originates at the beam–foil interaction point and shifts with it. The dataset shown in Fig. 4 was therefore repeated with a corrector magnet downstream of the BC displacing the beam on the foil. First preliminary evaluations show a clear shift of the emission pattern coinciding the corrector displacement. Centering and subtracting the two datasets isolates any shifting radiation pattern relative to each other. As the difference images do not show significant signal above the noise, this is an indication that the entire collected signal was shifted, yet SR and ER are not affected from the corrector operation. One possible explanation would be that TR clearly dominates the recorded signal pattern.

CONCLUSION

Coherent THz radiation from compressed electron bunches has been detected at FLUTE across four frequency channels from 272 to 925 GHz. A scan of RF phase and BC deflection reveals clear compression signatures, confirming that chirp and R_{56} can be matched to produce short bunches. The signal minimum observed in M4 indicates the shortest bunch of this campaign, with a bunch length in close proximity of the M4 coherence threshold of $\sigma_t \approx 172$ fs; for a better understanding, the data set will be reconstructed by beam-dynamics simulations. Transverse scans show half-moon intensity profiles as expected. An initial attempt to isolate TR from SR and ER by displacing the beam on the foil was carried out; the concept was demonstrated.

REFERENCES

[1] M. Nasse *et al.*, "First THz light generated in high energy section of FLUTE", in *Proc. IPAC'25*, Taipei, Taiwan, Jun. 2025, pp. 1186–1188. doi:10.18429/JACoW-IPAC2025-TUPM010

[2] M. J. Nasse *et al.*, "FLUTE: A versatile linac-based THz source", *Rev. Sci. Instrum.*, vol. 84, no. 2, p. 022705, Feb. 2013. doi:10.1063/1.4790431

[3] J. L. Steinmann *et al.*, "Continuous bunch-by-bunch spectroscopic investigation of the microbunching instability", *Phys. Rev. Accel. Beams*, vol. 21, no. 11, p. 110705, Nov. 2018. doi:10.1103/PhysRevAccelBeams.21.110705

[4] J. S. Nodvick and D. S. Saxon, "Suppression of coherent radiation by electrons in a synchrotron", *Phys. Rev.*, vol. 96, no. 1, pp. 180–184, Oct. 1954. doi:10.1103/PhysRev.96.180

[5] M. Schwarz *et al.*, "Comparison of Various Sources of Coherent THz Radiation at FLUTE", in *Proc. IPAC'12*, New Orleans, LA, USA, May 2012, pp. 568–570. doi:10.5445/IR/1000046483

[6] M. Schwarz *et al.*, "Computing coherent synchrotron radiation from Liénard-Wiechert potentials", in *Proc. IPAC'26*, Deauville, France, May 2026, paper WEP5080, 2026.

[7] C. Xu, E. Bründermann, A.-S. Müller, A. Santamaria Garcia, M. Schwarz, and J. Schäfer, "Optimization Studies of Simulated THz Radiation at FLUTE", in *Proc. IPAC'22*, Bangkok, Thailand, Jun. 2022, pp. 2292–2295. doi:10.18429/JACoW-IPAC2022-WEPOMS023

[8] J. Schäfer, "Lattice design of a transfer line for ultra-short bunches from flute to cstart", MA thesis, Karlsruher Institut für Technologie (KIT), Karlsruhe, Germany, 2019. doi:10.5445/IR/1000105061

[9] Wikipedia contributors, "Doughnut — wikipedia, the free encyclopedia", [Online; accessed 08-May-2026], 2026, https://en.wikipedia.org/wiki/Doughnut,